Heliyon xxx (xxxx) e29452

Contents lists available at ScienceDirect

Heliyon

journal homepage: www.elsevier.com/locate/heliyon

Research article

Synthesis, characterization, and optoelectronic properties of zinc oxide nanoparticles: A precursor as electron transport layer

Sunday Wilson Balogun [a], Hakeem Olayinka Oyeshola [b,*], Adegbenro Sunday Ajani [c], Olusola Oladele James [d], Mojoyinola Kofoworola Awodele [b], Hope Kofoworola Adewumi [b], George Atilade Àlàgbé [b], Olusegun Olabisi [e], Opeyemi Samson Akanbi [b], Festus Akintunde Ojeniyi [b], Yekinni Kolawole Sanusi [b]

[a] Department of Materials Science and Engineering, Kwara State University, P.M.B 1530. Malete, Nigeria
[b] Department of Pure and Applied Physics, Ladoke Akintola University of Technology, Ogbomoso, Nigeria
[c] Department of Physics and Material Science, Kwara State University, P.M.B 1530. Malete, Nigeria
[d] Department of Pure and Applied Chemistry, Kwara State University P.M.B 1530 Malete, Nigeria
[e] Department of Science Laboratory Technology, Ladoke Akintola University of Technology, Ogbomoso, Nigeria

CORRECTED PROOF

1. Introduction

The pressure on fossil fuel resources has intensified due to the world's unsustainable energy use, which has led to an increase in the effects of both climate change and global warming due to the release of greenhouse gases. Natural gas, oil, and coal have been shown to harm both the environment and human health (GHGs). Therefore, there is increasing global interest in alternative forms of energy. In comparison to traditional fossil fuels, sunlight is a particularly promising clean and widely available source [1,2]. Synthesis of metal oxide such as ZnO as a precursor with plant extract as a reducing agent to form nanoparticles for photovoltaic and electronics applications called for more research due to the issue of recombination associated with the solar cell that reduces their efficiency [3–16]. The recombination of electron-hole pair reduces power conversion efficiencies of photovoltaic devices hence a solution is needed to mitigate this flaw [17,18]. Published studies on the incorporation of semiconducting oxide such as Zinc oxide [18,19], zirconium [20], tellurium [21], selenium [22] TiO_2 and Cdse in solar cells as electron acceptors have been reported [23,24]. Synthesis of nanoparticles can be categorized into three forms biosynthesis, chemical and physical methods. The characteristic parameters of nanomaterial including, shape, size, dissolution, agglomeration state, chemical composition, specific surface area, crystal structure, surface morphology, surface energy, surface coating, and surface charge, impact biological interactions, fate, and the desired or adverse outcomes of nanomaterial [25]. However, the physical and chemical route of synthesis present some disadvantages such as high-energy requirements and hazards from chemicals used which result in environmental pollution and degradation [26,27]. The biosynthesis method was chosen because of its relative advantage over other techniques due to its low cost, low energy requirement, low pressure less hazardous and environment friendly [28] biocompatibility, sustainability, non-toxic reagents, enhanced stability, ease of process, and elimination of unnecessary processing during synthesis, whereas the physicochemical methods are quite expensive and may produce toxic by-products [21]. Report on the synthesis of ZnO.NP using Cordyline fruticosa extract for photovoltaic and electronic applications is rare in literature and the use of plant extracts affords the advantage of phytochemical acting as a reducing agent [29–31]. This study examines and evaluates extract from Cordyline fruticosa to produce zinc oxide nanoparticles via the green synthesis route for possible application as a window layer in optoelectronic applications.

* Corresponding author.
E-mail address: hooyeshola@lautech.edu.ng (H.O. Oyeshola).

https://doi.org/10.1016/j.heliyon.2024.e29452
Received 23 January 2024; Received in revised form 29 March 2024; Accepted 8 April 2024
2405-8440/© 20XX

Note: Low-resolution images were used to create this PDF. The original images will be used in the final composition.

2. Materials and methods

2.1. Materials

The materials used were zinc nitrate procured from Sigma-Aldrich. Other reagents such as ethanol (99.8 %), Isopropanol alcohol (IPA) and de-ionized water were purchased locally Cordyline fruticosa leaves were harvested in the environment.

2.2. Methods

2.2.1. Extraction procedure of Cordyline fruticosa leaf

30 g of fresh Cordyline fruticosa leaves were plucked from the main plant and washed with de-ionized water to remove impurities. The fresh leaves were air-dried at a temperature of 25 ± 2 °C for 20 days. The dried leaves were crushed and ground to powder particles thereafter 45.0 g of the powdered samples were added to 450 mL of boiled de-ionized water and stirred for 3 h at 40 °C. The mixed solution was left to cool under an ambient atmosphere. After this the solution was filtered and the process was repeated severally to get rid of organic residue.

2.2.2. Synthesis procedure

15.0 g of zinc nitrate considered a zinc precursor was dissolved in 150 mL solution extract of Cordyline fruticosa and homogeneously mixed by magnetic stirrer for 6 h without heat; there was a color change in the solution which was observed to be golden green. The product was sealed to reduce the photo-induced effect and left to precipitate at room temperature for 24 h. The slurry precipitate obtained was washed with de-ionized water and dried at 20 °C. The dried product powder was washed several times with de-ionized water and then annealed at 500 °C for 1h in a carbolite tubular furnace (Srw 21–501042 Type-CT17) and allowed to cool to room temperature to obtain powder ZnO.NP. To deposit ZnO.NP film over a clean glass substrate, ZnO.NP powder was dissolved in ethanol and deposited by spin-coating technique on a glass substrate surface at 3000 rpm for 30 s. The thickness of the film depends on the number of drops. 5 films were fabricated at various thicknesses which are, T_1 = 883.43 nm, T_2 = 2450.50 nm, T_3 = 3715.25 nm, T_4 = 4175.95 nm, and T_5 = 4625.35 nm. ZnO.NP thin films were baked for 10 min at 200 °C in the oven to dry up and the films were characterized.

2.3. Characterization of synthesized ZnO.NP

Characterization of deposited samples of synthesized ZnO.NP were carried out by UV–Vis spectrophotometer (ASUV-6300PC), X-ray diffraction (Rigaku Machine), FTIR (M530 FT-IR), Transmission Electron spectroscopy (JEM-ARM200F-G), Scanning Electron spectroscopy (JOEL-JSM 7600F), Electron Dispersive X-ray (EDX) and current-voltage (I–V) characteristic of synthesized ZnO.NP have been examined using Four Point Probe (4 PP) for current-voltage measurement.

3. Results and discussion

3.1. UV–visible spectroscopic analysis of synthesized NPs

The optical properties of the samples deposited were investigated with UV–Vis as shown in Fig. 1a is the value of optical transmittance at various thicknesses. T_4 has the lowest optical transmittance which translates to the highest optical absorbance in Fig. 1b. Fig. 1a and b shows ZnO.NP optical transmittance and absorbance as a function of different thicknesses namely, T_1 = 883.43 nm, T_2 = 2450.50 nm, T_3 = 3715.25 nm, T_4 = 4175.95 nm, and T_5 = 4625.35 nm. Observation of Fig. 1b shows T_4 = 4175.95 nm has maximum absorbance, which occurs at 1.40 over 346.4 nm.

3.1.1. Calculation of energy band gap

The plot of optical band-gap energy was done utilizing Tauc plot equation (1) [32].

$$(\alpha h\nu) = A(h\nu - Eg)^n \quad (1)$$

Where α is the optical absorption coefficient, h is Planck's constant, ν is the photon frequency, A is the equation constant related to the properties of the conduction and valence bands, n is the exponent factor and Eg is the energy between the bands. Regarding equation (1) n = ½ for allowed direct transitions and n = 2 for allowed indirect transition of unpaired electrons. $(\alpha h\nu)^2$ plot against photon energy ($h\nu$) is as shown in Fig. 2 calculated using Eq. (2)

$$\alpha = 2.303\left(\frac{A}{t}\right) \quad (2)$$

Where t is the film thickness and A is the absorbance.

CORRECTED PROOF

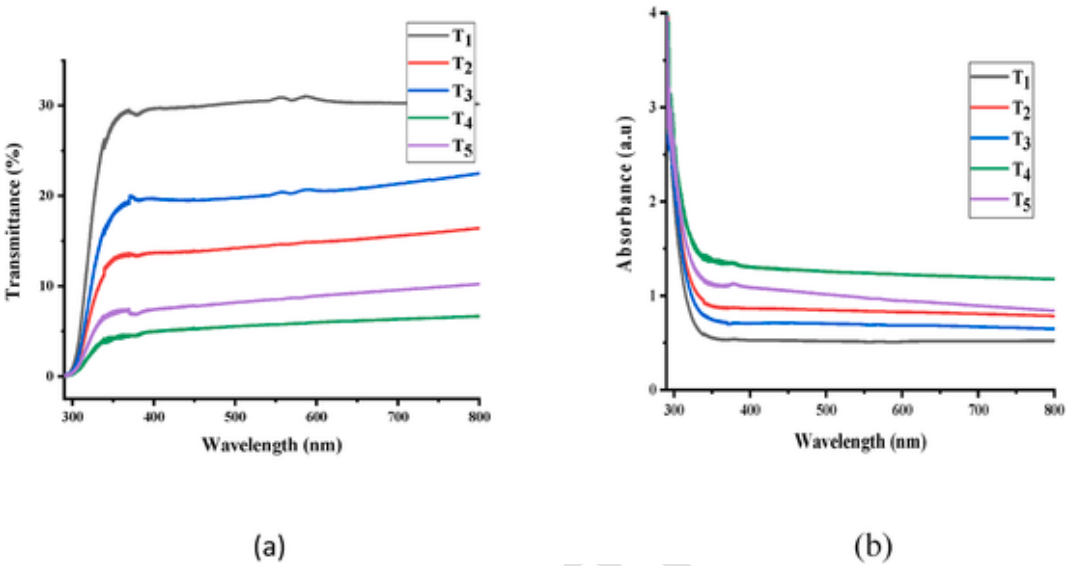


Fig. 1. (a) Optical percentage transmittance of ZnO.NP at different thicknesses. (b) Absorbance spectral of ZnO.NP at different thicknesses.

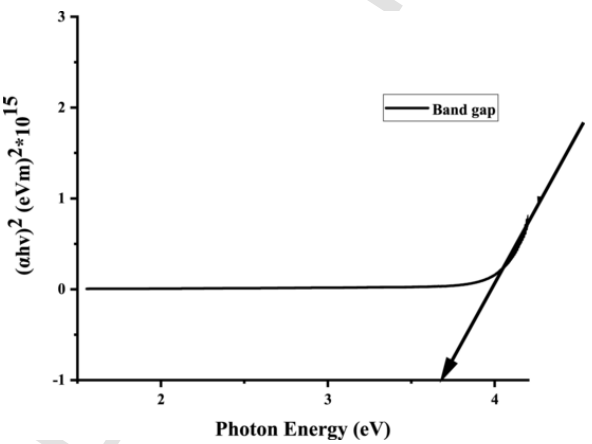


Fig. 2. Tauc's plot of energy band gap.

3.2. FTIR spectroscopy analysis

Shown in Fig. 3 is the characteristic absorption band peak at 3448.05 cm^{-1} is attributed to both asymmetric and symmetric stretching modes of the hydroxyl compound (Zn–OH). The spectroscopic absorption band peaks at 2900.16 cm^{-1}, 2627.74 cm^{-1}, and 2524.20 cm^{-1} can be assigned to O–H stretching and bending vibrations of adsorbed water. O–H bonds revealed proteins or phenolic compounds in the bio-reduction of Zn ions to ZnO.NP Cordyline fruticosa extract acts as reducing agent to produce ZnO.NP. The peak observed at 1819.99 cm^{-1} is due to C═C, C═O, C═N stretching vibrations. Peaks around 1437.18 cm^{-1}, 880.55 cm^{-1}, and 728.83 cm^{-1} can be attributed to Zn–O, Zn–OH and Zn–*O*–Zn stretching modes. The notable peaks observed at low wavenumber confirmed Zn–O bond in the synthesized NPs and Zn–O functional group are found at low wavenumber and the single bond region as tabulated in Table 1.

3.3. X-ray diffraction analysis

ZnO.NP crystal structure was studied with X-ray diffraction spectroscopy (XRD Rigaku). Fig. 4 shows the XRD analysis pattern of ZnO.NP proves the hexagonal wurtzite crystalline structure in nature. The pattern shows peaks at $2\theta = 32^0$, 34^0, 36^0, 47^0, 56^0, 63^0 and 68^0 having the sets of corresponding lattice plane. The crystal analysis result obtained showed good agreement with no 01–1136. The synthesized nanoparticle powder is void of peaks of unwanted impurities which suggest good quality ZnO NPs. A careful observation of Fig. 4 shows high crystallinity because the diffraction peaks are narrow and strong. Debby-Scherer formula Eq. (3) [33] was

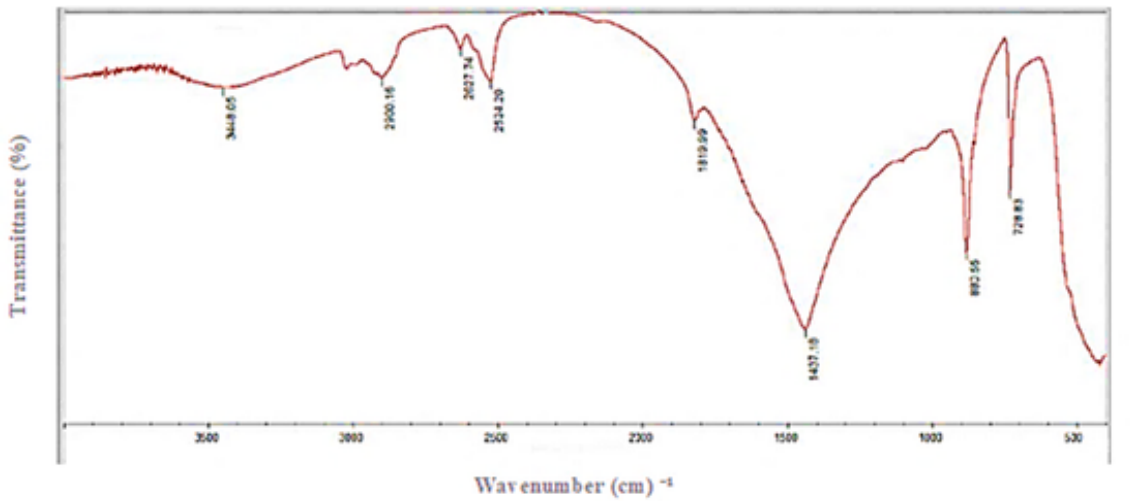


Fig. 3. FTIR spectrum of synthesized ZnO.NP.

Table 1
Absorption band and chemical bonds of ZnO.NP

Wave number (cm^{-1}) data obtained	Functional group
1437.18 cm^{-1}, 880.55 cm^{-1}, and 728.83 cm^{-1}	Zn–O single bond stretch, N–O stretch, Zn–OH.
1819.99 cm^{-1}	O–H bend, C═C, C═O, C═N double bonds, absorption caused by double bonds
3448.05 cm^{-1}, 2900.16 cm^{-1}, 2627.74 cm^{-1}, and 2524.20 cm^{-1}	O–H stretch, H-bonding, C–H stretch. Absorption caused by single bonds, characteristic for hydroxyl group (O–H).

Table 2
Zinc nanoparticles' electrical characteristics.

Sheet resistance (Ω)	Resistivity (Ωm^{-1})	Conductivity (Sm^{-1})
4349.03	110.47	9.1

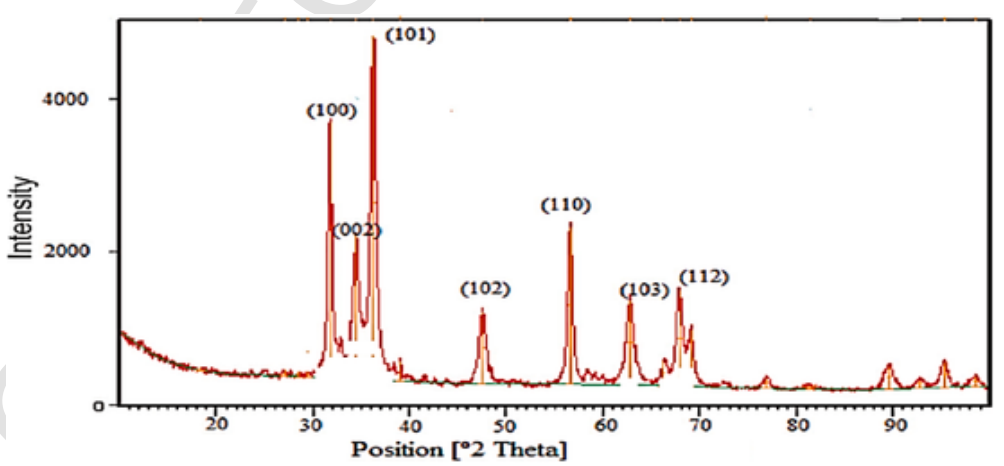


Fig. 4. XRD spectra of ZnO.NP.

used to calculate the estimated size of the NP which was determined to be 25 nm from the peak that corresponds to 36^0 at plane (101).

$$d = \frac{k\lambda}{\beta \cos \theta} \quad (3)$$

Where d is the average crystalline size, K is the Scherer constant; λ is radiation wavelength, where β and θ are peak and angle of diffraction (see). The crystallite size estimated concurs with the result reported by Safawo et al., [34].

3.4. SEM and TEM analyses

3.4.1. SEM analysis

Detailed information about ZnO.NP surface structure in Fig. 5 was provided by the SEM model (JOEL-JSM 7600F). The micrographs demonstrated by the NPs have crystalline form and hexagonal configuration [35].

3.4.2. Transmission electron microscopy analysis

Transmission electron microscopy analysis of synthesized ZnO.NP is shown in Fig. 6. The nanoparticle size was estimated in the range of 25–52 nm. This result was in agreement with the findings published by Sharmila et al., [36]. Both SEM and TEM analyses confirmed the formation of nanoparticles in the nanometer range.

3.5. EDX analysis

The electron dispersive X-ray (EDX) elemental composition per weight (%) of synthesized nanoparticles is shown in Fig. 7 Energy dispersive X-ray analysis confirmed the ZnO.NP formation with zinc weight of 64.2 % and Oxygen 12.0 % and the formation of nanoparticles was confirmed by EDX analysis in agreement with FTIR and XRD analysis.

PROOF

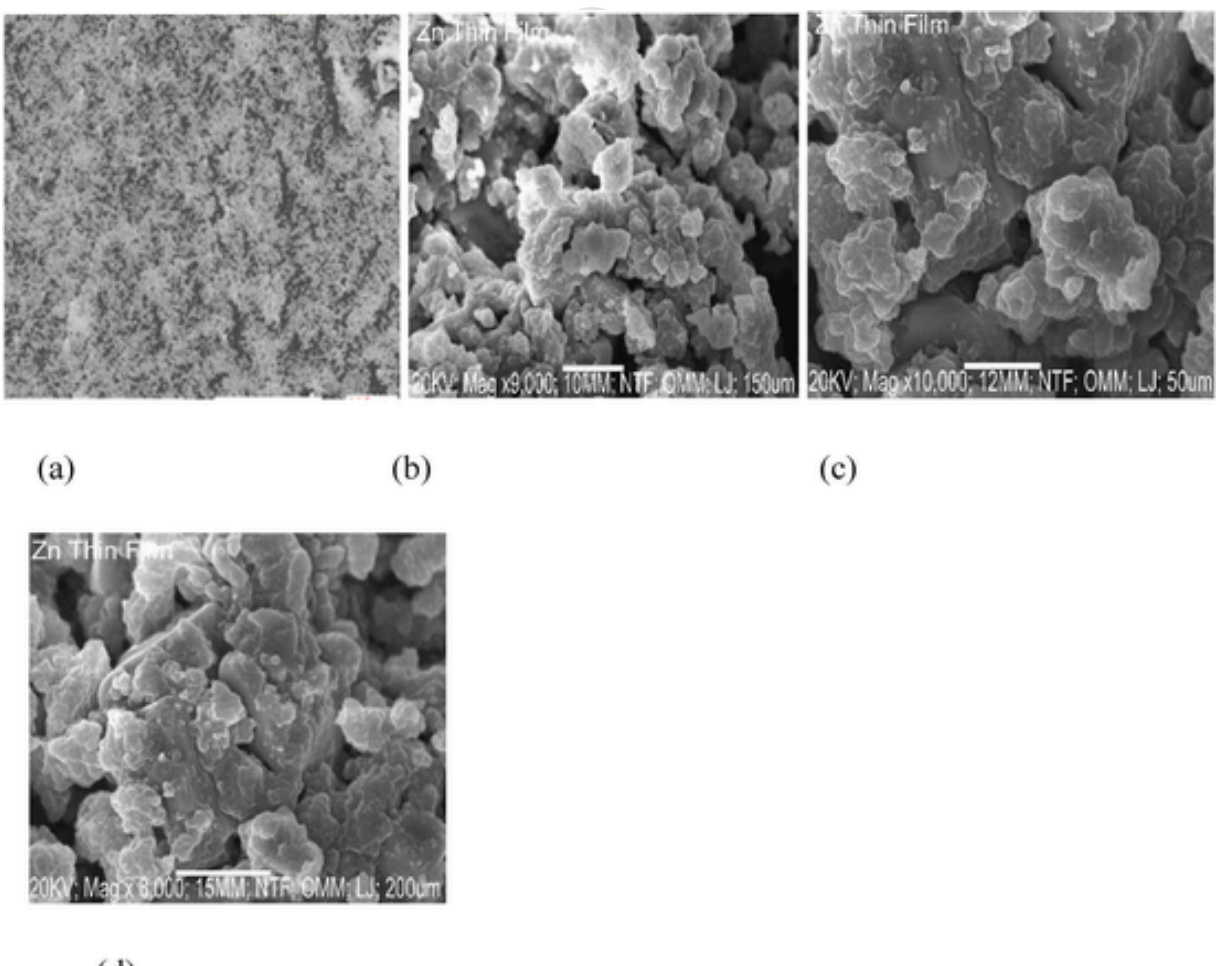


Fig. 5. SEM Images (a) Pure zinc oxide morphology and figures (b–d) Zinc oxide nanoparticles morphology at different magnifications.

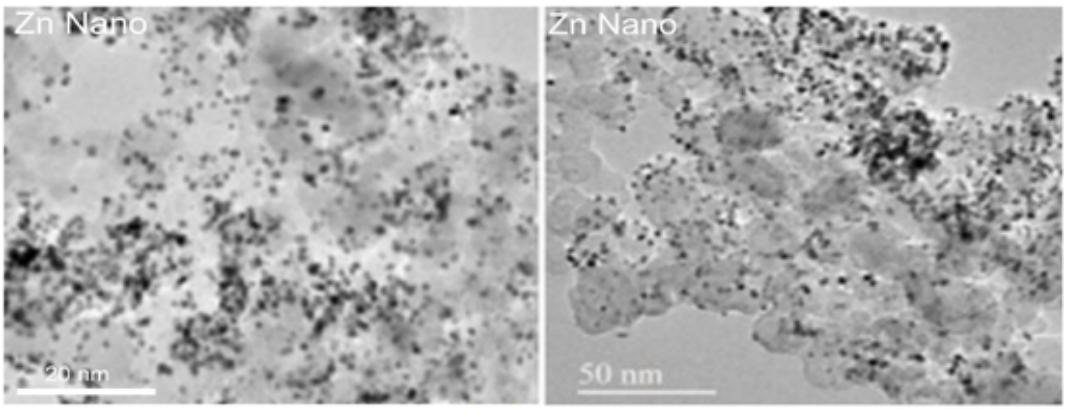


Fig. 6. (a, b): TEM Images of synthesized ZnO.NP at different magnifications.

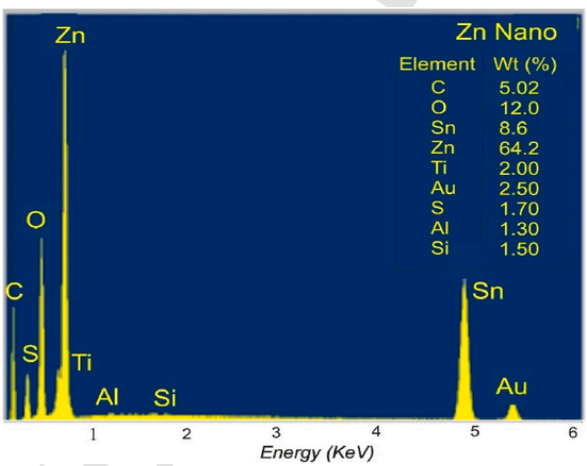


Fig. 7. EDX spectra of synthesized ZnO.NP.

3.6. Electrical properties determination

Zinc oxide nanoparticles' electrical behavior has been studied, assessed, and plotted in Fig. 8 using a four-point probes (4 PP) system equipped with Keithley2400 sources measuring unit. The current-voltage measurement was taken under ambient temperature.Sheet resistance was calculated with Eq. (4).

$$R_s = \frac{V}{I} \tag{4}$$

Where R_S = Sheet Resistance, V = Voltage, I = current.
Resistivity of ZnO.NP was computed with Eq. (5)

$$\rho = \frac{RA}{l} \tag{5}$$

Where ρ = Resistivity, R = Resistance, A = Area, L = length. Conductivity (σ) was computed using Eq. (6)

$$\sigma = \frac{1}{\rho} \tag{6}$$

4. Conclusions

The synthesis, characterization, and optoelectronic characteristics of ZnO.NP have been established, serving as an electron transport layer precursor. XRD analysis showed ZnO.NP hexagonal wurtzite structure with a high crystallinity. Scanning electron spec-

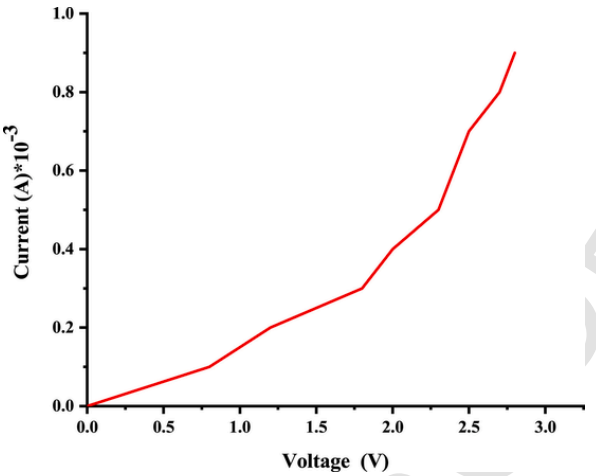


Fig. 8. Current-Voltage characteristics graph of ZnO.NP.

troscopy analysis revealed the hexagonal structure of ZnO.NP and crystalline properties. The electrical conductivity calculated showed improvement in the properties of ZnO.NP due to synthesis with Cordyline fruticosa extract. This result implies the properties of pure ZnO can be tuned or controlled by plant extract to reduce the electron recombination rate by injection of photoexcited electrons into the conduction band. Nanoparticles increase electron mobility which reduces the electron recombination rate by injection of photoexcited electron into the conduction band. Synthesized ZnO NPs will enhance solar cell performance because of the injection of excited electrons into the conduction band due to a reduction in electron recombination. These findings demonstrate the potential of one synthetic zinc oxide nanoparticle as an electron transport layer for solar cells and organic electronics applications. Production of nanoparticles with plant extract at low cost is visible and possible. Further work on the application of this research work on active polymer solar cells should be a subject of future research to ascertain its viability and efficiency.

CRediT authorship contribution statement

Sunday Wilson Balogun: Writing – review & editing, Writing – original draft, Methodology, Formal analysis, Conceptualization. **Hakeem Olayinka Oyeshola:** Writing – review & editing, Methodology. **Adegbenro Sunday Ajani:** Conceptualization. **Olusola Oladele James:** Writing – review & editing. **Mojoyinola Kofoworola Awodele:** Data curation, Visualization. **Hope Kofoworola Adewumi:** Data curation, Visualization. **George Atilade Àlàgbé:** Data curation, Formal analysis. **Olusegun Olabisi:** Data curation, Formal analysis, Investigation. **Opeyemi Samson Akanbi:** Investigation, Resources. **Festus Akintunde Ojeniyi:** Investigation, Visualization. **Yekinni Kolawole Sanusi:** Conceptualization, Supervision.

Declaration of competing interest

The authors declare no competing interests.

References

[1] O.A. Al-Shahri, F.B. Ismail, M.A. Hannan, M.H. Lipu, A.Q. Al-Shetwi, R.A. Begum, N.F. Al-Muhsen, E. Soujeri, Solar photovoltaic energy optimization methods, challenges and issues: a comprehensive review, J. Clean. Prod. 284 (2021) 125465.
[2] S. Yekinni, I. Asiata, O. Hakeem, L. Mubarak, Solar Photovoltaic Energy System, 2023.
[3] J.J. Marizcurrena, S. Castro-Sowinski, M.F. Cerdá, Improving the performance of dye-sensitized solar cells using nanoparticles and a dye produced by an Antarctic bacterium, Environmental Sustainability (2021) 1–11.
[4] P. Enciso, J.D. Decoppet, M. Grätzel, M. Wörner, F.M. Cabrerizo, M.F. Cerdá, A cockspur for the DSS cells: Erythrina crista-galli sensitizers, Spectrochim. Acta Mol. Biomol. Spectrosc. 176 (2017) 91–98.
[5] W. Ghann, H. Kang, T. Sheikh, S. Yadav, T. Chavez-Gil, F. Nesbitt, J. Uddin, Fabrication, optimization and characterization of natural dye sensitized solar cell, Sci. Rep. 7 (1) (2017) 41470.
[6] G. Calogero, A. Bartolotta, G. Di Marco, A. Di Carlo, F. Bonaccorso, Vegetable-based dye-sensitized solar cells, Chem. Soc. Rev. 44 (10) (2015) 3244–3294.
[7] G. Calogero, I. Citro, C. Crupi, G. Carini Jr, D. Arigò, G. Spinella, A. Bartolotta, G. Di Marco, Absorption spectra, thermal analysis, photoelectrochemical characterization and stability test of vegetable-based dye-sensitized solar cells, Opt. Mater. 88 (2019) 24–29.
[8] P. Hernández-Velasco, I. Morales-Atilano, M. Rodríguez-Delgado, J.M. Rodríguez-Delgado, D. Luna-Moreno, F.G. Ávalos-Alanís, J.F. Villarreal-Chiu, Photoelectric evaluation of dye-sensitized solar cells based on prodigiosin pigment derived from Serratia marcescens 11E, Dyes Pigments 177 (2020) 108278.
[9] H. Zhou, L. Wu, Y. Gao, T. Ma, Dye-sensitized solar cells using 20 natural dyes as sensitizers, J. Photochem. Photobiol. Chem. 219 (2–3) (2011) 188–194.
[10] S. Ananth, P. Vivek, T. Solaiyammal, P. Murugakoothan, Pre dye treated titanium dioxide nano particles sensitized by natural dye extracts of Pterocarpus marsupium for dye sensitized solar cells, Optik 126 (9–10) (2015) 1027–1031.
[11] P. Enciso, M. Woerner, M.F. Cerdá, Photovoltaic cells based on the use of natural pigments: phycoerythrin from red-antarctic algae as sensitizers for DSSC, MRS Advances 3 (61) (2018) 3557–3562.
[12] A. Lim, N. Haji Manaf, K. Tennakoon, R.L.N. Chandrakanthi, L.B.L. Lim, J.M.R. Bandara, P. Ekanayake, Higher performance of DSSC with dyes from Cladophora sp. as mixed cosensitizer through synergistic effect, Journal of Biophysics 2015 (2015).

CORRECTED PROOF

[13] A.L. Pinto, H. Cruz, J. Oliveira, P. Araújo, L. Cruz, V. Gomes, C.P. Silva, G.T. Silva, T. Mateus, G. Calogero, V. de Freitas, Dye-sensitized solar cells based on dimethylamino-π-bridge-pyranoanthocyanin dyes, Sol. Energy 206 (2020) 188–199.
[14] A.T. Khalil, M. Ovais, I. Ullah, M. Ali, Z.K. Shinwari, S. Khamlich, M. Maaza, Sageretia thea (Osbeck.) mediated synthesis of zinc oxide nanoparticles and its biological applications, Nanomedicine 12 (15) (2017) 1767–1789.
[15] K. Parveen, V. Banse, L. Ledwani, Green synthesis of nanoparticles: their advantages and disadvantages, in: AIP Conference Proceedings, vol. 1724, AIP Publishing, 2016, April 1.
[16] S.W. Balogun, O.O. James, Y.K. Sanusi, O.H. Olayinka, Green synthesis and characterization of zinc oxide nanoparticles using bashful (Mimosa pudica), leaf extract: a precursor for organic electronics applications, SN Appl. Sci. 2 (2020) 1–8.
[17] H. Xu, H. Zhang, Y. Ma, M. Jiang, Y. Zhang, Y. Wu, H. Zhang, R. Xia, Q. Niu, X.A. Li, W. Huang, Morphology control of organic halide perovskites by adding BiFeO3 nanostructures for efficient solar cell, Sci. Rep. 9 (1) (2019) 15441.
[18] Biosynthesis of Zinc oxide nanoparticles using Bergenia ciliate aqueous extract and evaluation of their photocatalytic and antioxidant potential. Inorg. Chem. Commun., 134, 109020.
[19] G.A. Rather, A. Nanda, M.A. Pandit, S. Yahya, H. Barabadi, M. Saravanan, Biosynthesis of Zinc oxide nanoparticles using Bergenia ciliate aqueous extract and evaluation of their photocatalytic and antioxidant potential, Inorg. Chem. Commun. 134 (2021) 109020.
[20] A.R.G. Ghomi, M. Mohammadi-Khanaposhti, H. Vahidi, F. Kobarfard, M.A.S. Reza, H. Barabadi, Fungus-mediated extracellular biosynthesis and characterization of zirconium nanoparticles using standard penicillium species and their preliminary bactericidal potential: a novel biological approach to nanoparticle synthesis, Iran. J. Pharm. Res. (IJPR): IJPR 18 (4) (2019) 2101.
[21] H. Vahidi, F. Kobarfard, A. Alizadeh, M. Saravanan, H. Barabadi, Green nanotechnology-based tellurium nanoparticles: exploration of their antioxidant, antibacterial, antifungal and cytotoxic potentials against cancerous and normal cells compared to potassium tellurite, Inorg. Chem. Commun. 124 (2021) 108385.
[22] H. Vahidi, F. Kobarfard, Z. Kosar, M.A. Mahjoub, M. Saravanan, H. Barabadi, Mycosynthesis and characterization of selenium nanoparticles using standard penicillium chrysogenum PTCC 5031 and their antibacterial activity: a novel approach in microbial nanotechnology, Nanomed. J 7 (4) (2020) 315–323.
[23] A.P. Wanninayake, S. Gunashekar, S. Li, B.C. Church, N. Abu-Zahra, CuO nanoparticles based bulk heterojunction solar cells: investigations on morphology and performance, J. Sol. Energy Eng. 137 (3) (2015) 031016.
[24] W.J. Beek, M.M. Wienk, R.A. Janssen, Efficient hybrid solar cells from zinc oxide nanoparticles and a conjugated polymer, Adv. Mater. 16 (12) (2004) 1009–1013.
[25] H. Samadian, M.S. Salami, M. Jaymand, A. Azarnezhad, M. Najafi, H. Barabadi, A. Ahmadi, Genotoxicity assessment of carbon-based nanomaterials; Have their unique physicochemical properties made them double-edged swords? Mutat. Res. Rev. Mutat. Res. 783 (2020) 108296.
[26] A. Diallo, B.D. Ngom, E. Park, M. Maaza, Green synthesis of ZnO nanoparticles by Aspalathus linearis: structural & optical properties, J. Alloys Compd. 646 (2015) 425–430.
[27] K. Parveen, V. Banse, L. Ledwani, Green synthesis of nanoparticles: their advantages and disadvantages, in: AIP Conference Proceedings, vol. 1724, AIP Publishing, 2016, April 1.
[28] A. Thakur, N. Sharma, M. Bhatti, M. Sharma, A.V. Trukhanov, S.V. Trukhanov, L.V. Panina, K.A. Astapovich, P. Thakur, Synthesis of barium ferrite nanoparticles using rhizome extract of Acorus calamus: characterization and its efficacy against different plant phytopathogenic fungi, Nano-Structures & Nano-Objects 24 (2020) 100599.
[29] J. Yang, G. Liu, J. Lu, Y. Qiu, S. Yang, Electrochemical route to the synthesis of ultrathin ZnO nanorod/nanobelt arrays on zinc substrate, Appl. Phys. Lett. 90 (10) (2007).
[30] M. Maaza, Natural dyes for photonics applications, Novel plant bioresources: Applications in food, medicine and cosmetics (2014) 479–493.
[31] S.W. Balogun, S.A. Bello, H.O. Oyeshola, Influence of annealing temperature on the optical, morphological, structural, and electrical properties of zinc oxide thin film as a transparent conductive oxide electrode material nano plus, Sci. Tech. Nanomat. 2 (2) (2021) 2782–8174.
[32] J. Tauc, Optical properties of amorphous semiconductors, in: Amorphous and Liquid Semiconductors, Springer US, Boston, MA, 1974, pp. 159–220.
[33] A.L. Patterson, The Scherrer formula for X-ray particle size determination, Phys. Rev. 56 (10) (1939) 978.
[34] T. Safawo, B.V. Sandeep, S. Pola, A. Tadesse, Synthesis and characterization of zinc oxide nanoparticles using tuber extract of anchote (Coccinia abyssinica (Lam.) Cong.) for antimicrobial and antioxidant activity assessment, Open 3 (2018) 56–63.
[35] S.W. Balogun, H. Oyeshola, A.B. Kamil, S.K. Yekinni, G.R. Fajinmi, Evaluation of Photovoltaic Properties of Green Synthesized Zinc Oxide Nanoparticles from Extract of Carica Papaya for Anode Buffer Film Layer of Polymer Solar Cells, Available at: SSRN 4070949, 2022.
[36] G. Sharmila, C. Muthukumaran, K. Sandiya, S. Santhiya, R.S. Pradeep, N.M. Kumar, N. Suriyanarayanan, M. Thirumarimurugan, Biosynthesis, characterization, and antibacterial activity of zinc oxide nanoparticles derived from Bauhinia tomentosa leaf extract, Journal of Nanostructure in Chemistry 8 (2018) 293–299.

CORRECTED PROOF